Electrohydrodynamic drying of multiple food products: evaluating the potential of emitter-collector electrode configurations for upscaling

Thijs Defraeye [a,b,c], A. Martynenko[d]

[a] *Empa, Swiss Federal Laboratories for Materials Science and Technology, Laboratory for Biomimetic Membranes and Textiles, Lerchenfeldstrasse 5, 9014 St. Gallen, Switzerland*

[b] *Empa, Swiss Federal Laboratories for Materials Science and Technology, Multiscale Studies in Building Physics, Überlandstrasse 129, 8600 Dübendorf, Switzerland*

[c] *Chair of Building Physics, ETH Zurich, Stefano-Franscini-Platz 5, 8093 Zürich, Switzerland*

[d] *Department of Engineering, Dalhousie University, Agricultural Campus PO Box 550 Truro, Canada*

Keywords: Electro-aerodynamic; computational fluid dynamics; dehydration; airflow; corona discharge; COMSOL

Corresponding author

- E-mail thijs.defraeye@empa.ch
- Tel. +41 (0)58 765 4790

Abstract

Electrohydrodynamic (EHD) drying is a promising, non-thermal drying technology, based on ionic wind generation between an emitter and a collector electrode. This simulation-based study evaluates impact of various emitter-collector configurations for EHD drying in order to assess their potential towards industrial upscaling. The conventional wire-to-plate configuration, which creates impinging flow, is found not to be an optimal solution for EHD drying of multiple food products in a fast and uniform way. With a single wire (emitter), it is found that the products placed more downstream dry slower due to the progressive loading of the air with water vapor. With multiple emitters, up to a threefold increase in drying time of the food products is found, compared to a single wire. This increase is caused by the recirculation of most air. To avoid moisture accumulation in the drying zone, a wire-to-mesh configuration is proposed. The mesh collector minimizes interference of neighboring airflows and avoids recirculation of moist air in the drying zone. As such, the wire-to mesh configuration provides more uniform drying between adjacent products, but also within a product, as it can dry from all its surfaces. An increase in emitter density for the wire-to-mesh configuration leads to an overall increase in airspeed, but surprisingly not to increased product drying rates. The reason is that the high-speed EHD airflow is always generated very locally in the vicinity of the emitter and collector. Thereby the convective drying process is not affected so much by the emitter density.

Introduction

Electrohydrodynamic (EHD) drying is a non-thermal technology where ionic wind is created in order to improve the dehydration of heat-sensitive materials, predominantly food products (Bai et al., 2013; Martynenko and Zheng, 2016; Pirnazari et al., 2016; Singh et al., 2015; Taghian Dinani and Havet, 2015). A high voltage in the kilovolt range is imposed between an emitter and collector electrode, which induces corona discharge, so local ionization of the air, at the emitter. The movement of the ions towards the collector and their resulting collisions with air molecules lead to a net air movement. EHD drying is reported to reduce drying time and product shrinkage, to enhance rehydration capacity, to improve texture and to better preserve color, flavor and nutritional value (Bai et al., 2013; Ding et al., 2015; Esehaghbeygi et al., 2014; Esehaghbeygi and Basiry, 2011; Taghian Dinani et al., 2015, 2014; Yang and Ding, 2016). This promising alternative drying technology has been investigated for almost three decades, including by laboratory-scale tests (Barthakur, 1990; Chen et al., 1994; Hashinaga et al., 1999; Isobe et al., 1999), and working small-scale prototypes have been built (Lai, 2010). Nevertheless, EHD dryers are not commercially available yet, to our best knowledge.

The step towards industrial upscaling is hindered, amongst others, by the fact that most of the aforementioned studies focused on EHD drying of a single sample, using a wire/needle-to-plate configuration (Defraeye and Martynenko, 2017). This sample was a single product or several small products (e.g. berries) spaced together to form one entity. Only rarely, multiple individual products were dried together (Taghian Dinani and Havet, 2015). In this case, effects of product spacing and heterogeneity on the drying rate have not been investigated. Industrial processes however require the simultaneous drying of large amounts of products. When using the wire/needle-to-plate configuration for this purpose, upscaling problems can occur (Defraeye and Martynenko, 2017). For a single wire-to-plate configuration (Figure 1a), it is probably difficult to achieve a uniform drying rate for multiple food products, located at different distances from the emitter. An EHD-driven air jet is directed towards the plate and is then diverted to the sides over the products. When air passes over successive products, partial saturation of the air with vapor will occur. This will likely reduce the drying rate of products more downstream, but this effect was not quantified yet. For a multiple wire-to-plate configuration (Figure 1b), another problem arises due to the multiple air jets that bounce back from the product: partial saturation of the recirculating air with vapor will occur, which can also slow down the drying rate.

A better insight in the impact of the emitter-collector electrode configuration and spacing between multiple products on their drying rate and heterogeneity is required to enable further industrial upscaling. As a step towards drying large amounts of products faster and more uniform by means of

EHD, this simulation-based study evaluates several configurations (Figure 1). These include the conventional wire-to-plate configuration and the alternative wire-to-mesh configuration.

Materials and Methods

The computational model, boundary conditions and simulation parameters are presented in detail in a previous study (Defraeye and Martynenko, 2018), and therefore only the main features are highlighted here. The 2D continuum, finite-element model calculates convective EHD drying of rectangular apple fruit slices (L x H = 10 x 5 mm). Airflow is generated by placing a high voltage difference between a cylindrical wire (V_w = 20 kV, with radius r_w = 250 µm), i.e. the emitter electrode, and a grounded collector electrode, spaced at a distance d_{ec} = 20 mm. Under this electrostatic action, airflow is generated, which draws air at a temperature (T_{ref}) of 20 °C and a relative humidity (RH_{ref}) of 30% from the inlet towards the fruit to be dried. Multiple food products are spaced at a distance w_p. Three configurations of emitter-collector electrodes are evaluated for EHD drying (Figure 1):

- (a) Impinging flow for a single wire-to-plate configuration, so where a single EHD air jet is generated. This case is evaluated for w_p = 1.5 L, 3L, 4.5L, 6L. As the size of the zone where the products are placed in is 30L, in total 19, 9, 7 and 5 products are included in the model, respectively. The width of the domain is extended to 60L to avoid an impact of the lateral boundaries on the drying process.
- (b) Impinging flow for a periodic wire-to-plate configuration, where an EHD air jet is generated above each individual fruit. This case is evaluated for w_p = 4L, 6L, 8L, 10L, 15L, 20L, 25L, 30L.
- (c) Flow around the products for a periodic wire-to-mesh configuration, where an EHD air jet is generated above each individual fruit. This case is evaluated for following w_p = 4L, 6L, 8L, 10L, 15L, 20L, 25L, 30L.

Note that for the two last cases, periodic boundary conditions are used, so only a single product needed to be explicitly modelled.

The computational model solves for (1) the electrostatic potential field, (2) the associated charge transport due to ion drift, caused by the corona discharge, (3) the resulting airflow generation due to ion movement and collision with neutral air molecules, (4) heat and mass transport in the fruit tissue due to convective, EHD-generated, airflow, which leads to dehydration. Airflow is coupled to the electrostatic field by a volumetric source term in the Navier-Stokes equations for turbulent flow, namely the Coulomb force. Out of the airflow calculation, the convective heat and mass transfer coefficients (CHTC and CMTC) are determined. These convective transfer coefficients are imposed afterwards on the product surface in order to calculate the impact of the airflow field on the fruit

dehydration process. This model is implemented in COMSOL Multiphysics (version 5.2a), which is a finite-element based commercial software. The computational grid, time step, tolerances for convergence and other solver settings are determined from sensitivity analysis. The electrical potential and space charge density are solved using linear shape functions together with a fully-coupled direct solver, relying on the MUMPS (MUltifrontal Massively Parallel sparse direct Solver) solver scheme. Turbulent airflow is solved using a segregated solver, relying on the PARDISO (PARallel DIrect sparse SOlver Interface) solver scheme. The drying process is solved using quadratic shape functions, together with a fully coupled direct solver, relying on the MUMPS solver scheme.

To compare drying efficiencies, the critical drying time (t_{crit}) is used (Defraeye and Verboven, 2017). It is the time needed for the sample to reach the critical moisture content (w_{crit}). The latter is defined as the (volume-)averaged moisture content in the sample that corresponds, via the sorption isotherm, to an equilibrium water activity $a_{w,crit}$ = 0.6, below which no spoilage occurs. For the present study, w_{crit} is 37.8 kg m^{-3}, leading to a critical dry-base moisture content (X_{crit}) of 0.29 kg kg$_{dm}^{-1}$. With t_{crit}, each drying curve (X vs. time) can be characterized by a single value, which simplifies quantitative comparison of drying kinetics of different products. Note that all the used submodels for EHD, the associated airflow and the drying process were validated previously, and a verification of the EHD model with experimental and analytical data was presented as well (Defraeye and Martynenko, 2018).

Results and Discussion

Single wire-to-plate (impinging flow)

The results for 4 product spacings are shown in Figure 2, namely the dry-matter moisture content (X), the CHTC for each individual fruit and its critical drying time. The CHTCs are used here to characterize the convective transfer rates, as the CMTCs were derived directly from the CHTCs using the heat and mass transfer analogy (Defraeye and Martynenko, 2018).

From Figure 2, it is clear that fruits dry progressively slower when they are further away (larger d_x) from the emitter, meaning they have a higher t_{crit} and a lower CHTC. The reason is that the air is progressively loaded with water vapor, from the dehydrating fruits, when moving away from the center to the sides of the domain. This more humid air induces lower convective transfer rates. There are two exceptions. The fruit below the emitter (nr. 1 in Figure 1) dries a bit slower than the subsequent fruit (nr. 2 in Figure 1). This is caused by the lower air speeds just below the emitter, which create a kind of stagnation zone. The last fruit in the row for w_p = 1.5L, namely nr. 10, dries about as fast as the previous one (nr. 9). Its trailing edge is not exposed to the recirculation zone of the subsequent fruit, in

which typically lower air speeds and convective transfer rates are present. In other words, the last fruit is less sheltered and can thereby dry faster.

In this study, differences in drying times (t_{crit}) of 24% (≈ 6 h) between the fastest and slowest drying fruit were found (for w_p = 1.5L), which will become even more pronounced if larger amounts of products are dried. As such, the well-researched single wire-to-plate configuration is clearly not suitable for industrial upscaling.

Periodic wire-to-plate (impinging flow)

The simulation results for impinging flow with a periodic wire-to-plate configuration are shown in Figure 3 (in red) for several product spacings w_p. The CHTC for each individual fruit and its critical drying time both significantly depend on the spacing between products (w_p). Increasing the spacing (w_p) results in a steep increase in CHTC and decrease in drying time. As air recirculates and becomes partially saturated with vapor in the vicinity of the product, the convective transfer coefficients (CTCs) are reduced and moisture removal from the products is slowed down. An asymptote in minimal drying time (≈ 16 h) is reached at large product spacings (> 150 mm). Using an product spacing of 4L increases the drying time to about 49h, which is three times larger than the minimal value at w_p = 30L (=300 mm). Since small product spacings will be essential in the wire-to-plate configuration to limit the size of EHD dryer, this configuration is not recommended for use in an industrial context.

Periodic wire-to-mesh (flow around product)

The results for flow around a product with a periodic wire-to-mesh configuration are shown in Figure 3 (in black) for several product spacings w_p. The average air speed at the domain inlet as a function of w_p is shown in Figure 4. The inverse proportional relation $U = f(w_p)$ is also shown (grey line), namely $U = a_x/w_p$, where a_x is a constant. This relation indicates that decreasing the wire spacing, thus also the product spacing in the present model, with a factor 2, doubles the average air speed. The aim is to evaluate the validity of this intuitive proportional relation, namely that if by increasing wire density, the average EHD generated airflow rate increases accordingly. The constant a_x is calibrated at the midpoint w_p = 15L (150 mm), with a_x = 78.

By increasing the density of the wires, the average air speed clearly increases in a non-linear way. By comparison with the analytical relation (grey line), the increase in speed is almost proportional to the decrease in w_p, except at low w_p (<10L). This means that if the density of the emitters is increased, the average air speed increases almost proportionally.

Surprisingly, the CHTC and the drying rate of the product do not increase significantly with this increase in speed, and remain almost constant for all product spacings. The main reason is that EHD airflow generation occurs always very local, in the vicinity of the emitter. This leads to high air speeds around the product, which are not that affected by the product spacing. In other words, by placing an emitter above the product, a very localized airflow field is generated. This interesting finding for upscaling means that placing the products and emitters closer together induces higher air speeds but not necessarily much higher drying rates.

In any case, the wire-to-mesh configuration minimizes interference of neighboring airflows and avoids recirculation of moist air in drying zone. Thereby, it provides more uniform drying between adjacent

products, but also within a product, as it can dry from all its surfaces. This major finding opens opportunity for industrial upscaling of EHD dryer by placing of multiple food products on the mesh collector.

Outlook

This study identifies that the conventional wire-to-plate configuration with impinging flow, despite being the most studied, is not an optimal solution to dry large amounts of food products in a fast and uniform way. The alternative wire-to-mesh configuration shows a better potential for industrial upscaling with the additional advantage that products can dry uniformly from all their surfaces. Such simulation-based studies enable a swift evaluation of the EHD drying process. This can speed up the design and optimization of EHD dryers.

Acknowledgements

We acknowledge the support of the World Food System Center (WFSC) of ETH Zürich.

References

Bai, Y., Qu, M., Luan, Z., Li, X., Yang, Y., 2013. Electrohydrodynamic drying of sea cucumber (Stichopus japonicus). LWT - Food Sci. Technol. 54, 570–576. doi:10.1016/j.lwt.2013.06.026

Barthakur, N., 1990. Electrohydrodynamic from NaCl solutions enhancement of evaporation. Desalination 78, 455–465. doi:http://dx.doi.org/10.1016/0011-9164(90)80064-I

Chen, Y., Barthakur, N.N., Arnold, N.P., 1994. Electrohydrodynamic (EHD) drying of potato slabs. J. Food Eng. 23, 107–119. doi:10.1016/0260-8774(94)90126-0

Defraeye, T., Blocken, B., Carmeliet, J., 2012. Analysis of convective heat and mass transfer coefficients for convective drying of a porous flat plate by conjugate modelling. Int. J. Heat Mass Transf. 55, 112–124. doi:10.1016/j.ijheatmasstransfer.2011.08.047

Defraeye, T., Martynenko, A., 2018. Electro-aerodynamic drying of food: new insights from conjugate modelling. J. Clean. Prod.

Defraeye, T., Martynenko, A., 2017. Future perspectives for electro-hydrodynamic drying of biomaterials. Dry. Technol. (accepted).

Defraeye, T., Verboven, P., 2017. Convective drying of fruit: Role and impact of moisture transport properties in modelling. J. Food Eng. 193, 95–107. doi:10.1016/j.jfoodeng.2016.08.013

Ding, C., Lu, J., Song, Z., 2015. Electrohydrodynamic drying of carrot slices. PLoS One 10, 1–12. doi:10.1371/journal.pone.0124077

Esehaghbeygi, A., Basiry, M., 2011. Electrohydrodynamic (EHD) drying of tomato slices (Lycopersicon esculentum). J. Food Eng. 104, 628–631. doi:10.1016/j.jfoodeng.2011.01.032

Esehaghbeygi, A., Pirnazari, K., Sadeghi, M., 2014. Quality assessment of electrohydrodynamic and microwave dehydrated banana slices. LWT - Food Sci. Technol. 55, 565–571. doi:10.1016/j.lwt.2013.10.010

Hashinaga, F., Bajgai, T.R., Isobe, S., Barthakur, N.N., 1999. Electrohydrodynamic (Ehd) drying of apple slices. Dry. Technol. 17, 479–495. doi:10.1080/07373939908917547

Isobe, S., Barthakur, N.N., Yoshino, T., Okushima, L., Sase, S., 1999. Electrohydrodynamic characteristics of agar gel. Food Sci. Technol. Res. 5, 132–136.

Lai, F.C., 2010. A prototype of EHD-enhanced drying system. J. Electrostat. 68, 101–104. doi:10.1016/j.elstat.2009.08.002

Martynenko, A., Zheng, W., 2016. Electrohydrodynamic drying of apple slices: Energy and quality aspects. J. Food Eng. 168, 215–222. doi:10.1016/j.jfoodeng.2015.07.043

Pirnazari, K., Esehaghbeygi, A., Sadeghi, M., 2016. Modeling the electrohydrodynamic (EHD) drying of banana slices. Int. J. Food Eng. 12, 17–26. doi:10.1515/ijfe-2015-0005

Singh, A., Vanga, S.K., Nair, G.R., Gariepy, Y., Orsat, V., Raghavan, V., 2015. Electrohydrodynamic drying (EHD) of wheat and its effect on wheat protein conformation. LWT - Food Sci. Technol. 64, 750–758. doi:10.1016/j.lwt.2015.06.051

Taghian Dinani, S., Hamdami, N., Shahedi, M., Havet, M., 2015. Quality assessment of mushroom slices dried by hot air combined with an electrohydrodynamic (EHD) drying system. Food Bioprod. Process. 94, 572–580. doi:10.1016/j.fbp.2014.08.004

Taghian Dinani, S., Havet, M., 2015. Effect of voltage and air flow velocity of combined convective-electrohydrodynamic drying system on the physical properties of mushroom slices. Ind. Crops Prod. 70, 417–426. doi:10.1016/j.indcrop.2015.03.047

Taghian Dinani, S., Havet, M., Hamdami, N., Shahedi, M., 2014. Drying of mushroom slices using hot air combined with an electrohydrodynamic (EHD) drying system. Dry. Technol. 32. doi:10.1080/07373937.2013.851086

Yang, M., Ding, C., 2016. Electrohydrodynamic (EHD) drying of the Chinese wolfberry fruits. Springer Plus 5, 909–929. doi:10.1186/s40064-016-2546-1

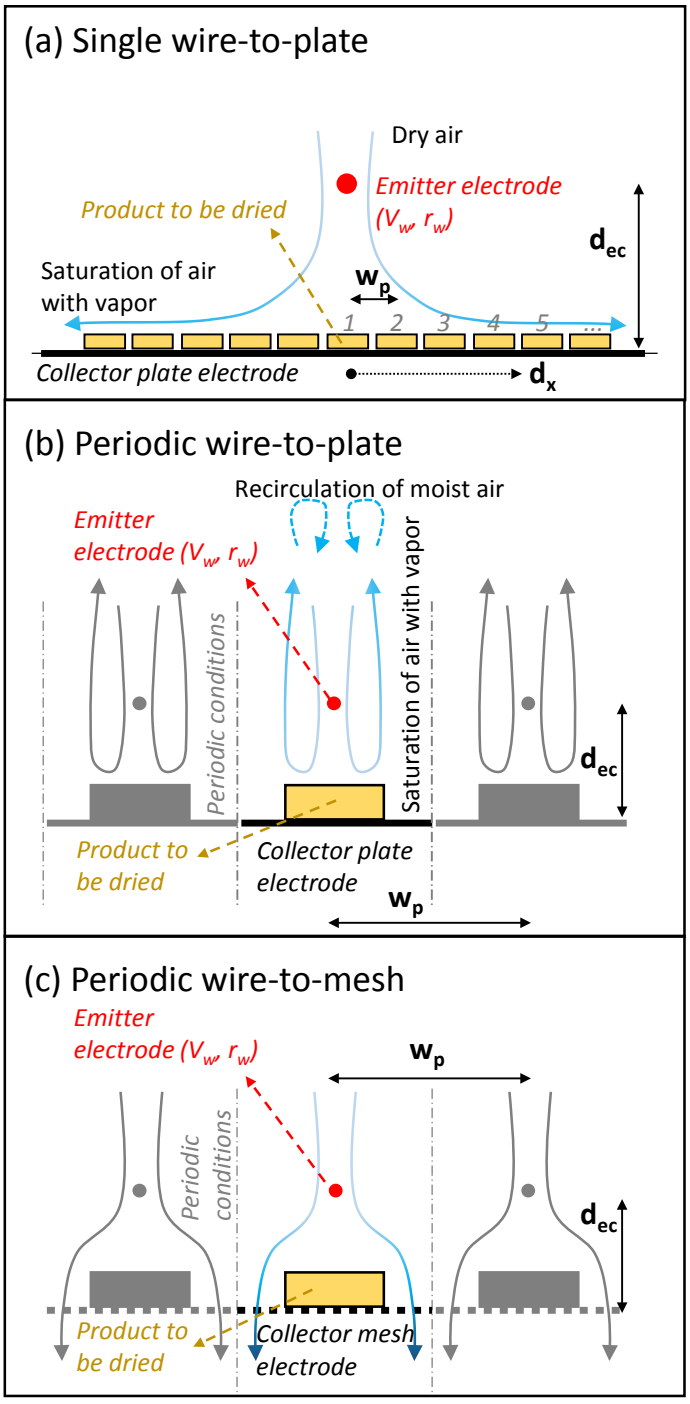

Figure 1. Types of configurations for EHD drying of multiple products: (a) impinging flow for a single wire-to-plate configuration, (b) impinging flow for a periodic wire-to-plate configuration, (c) flow around the products for a periodic wire-to-mesh configuration. (emitter = red, collector = black; periodic conditions indicate that multiple products are placed sideways; not to scale).

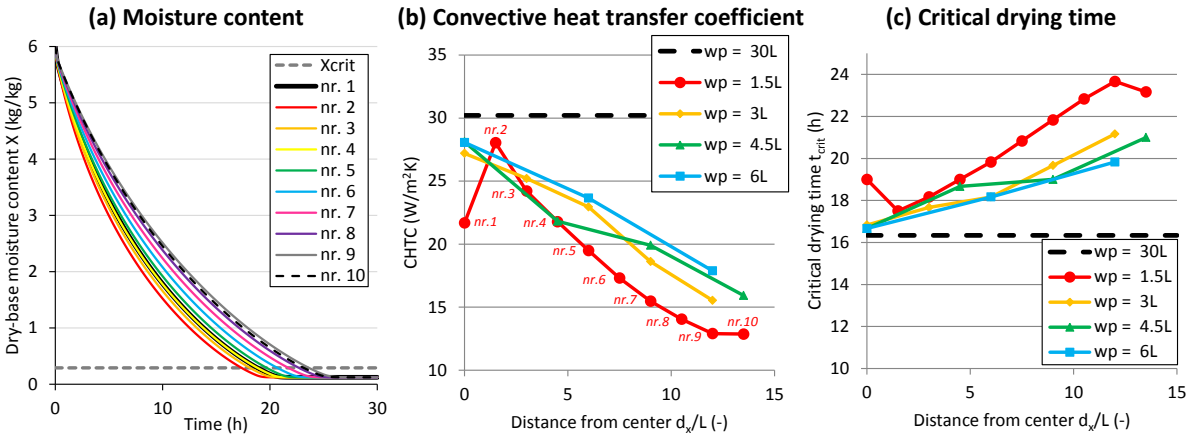

Figure 2. Impinging flow for a single wire-to-plate configuration: (a) dry matter moisture content (X) over time for each individual fruit for w_p = 1.5L; (b) the surface-averaged CHTC for each individual fruit as a function of the distance of the product from the centre d_x/L (emitter) for different w_p; (c) the critical drying time for each individual fruit as a function of d_x/L for different w_p. In (b), the results for a very large product spacing (w_p = 30L) are also indicated by the horizontal dashed black line.

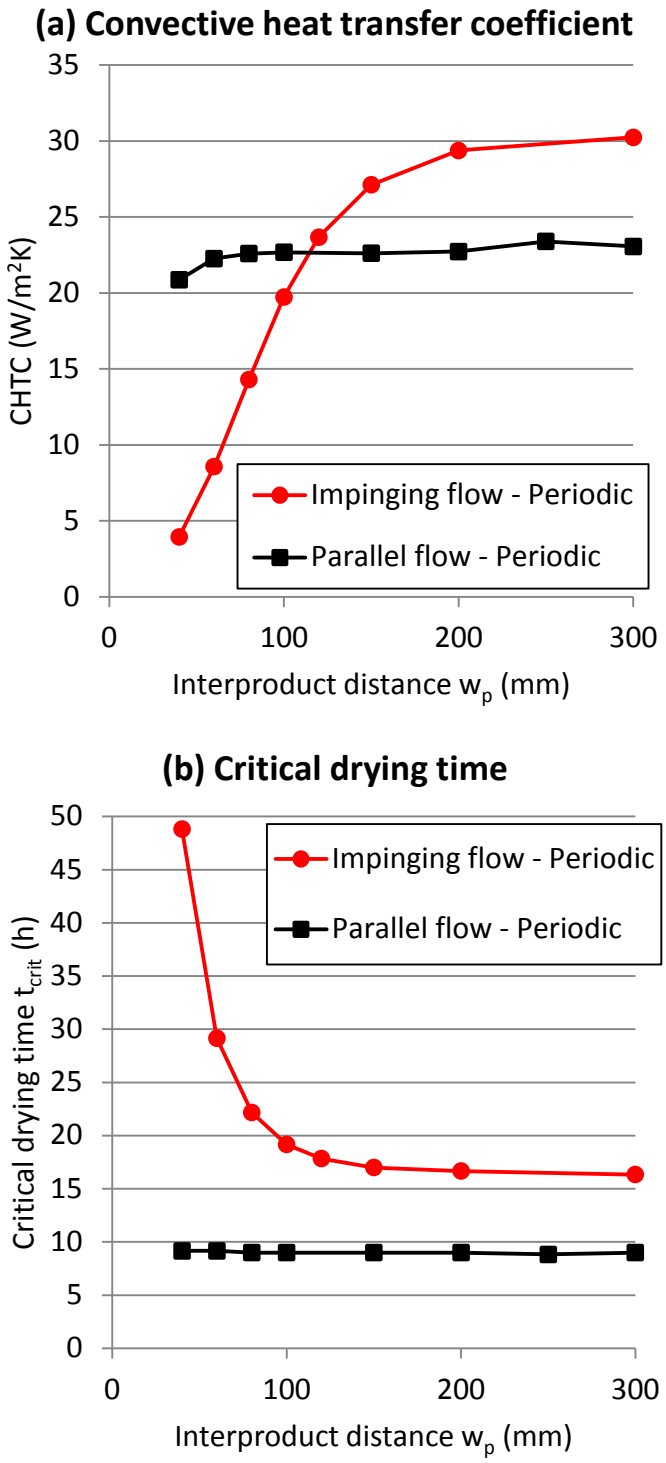

Figure 3. Impinging flow for a periodic wire-to-plate configuration and flow around a product (parallel flow) for a periodic wire-to-mesh configuration, calculated for variable product spacings w_p: (a) surface-averaged CHTC for each individual fruit; (b) critical drying time for each individual fruit.

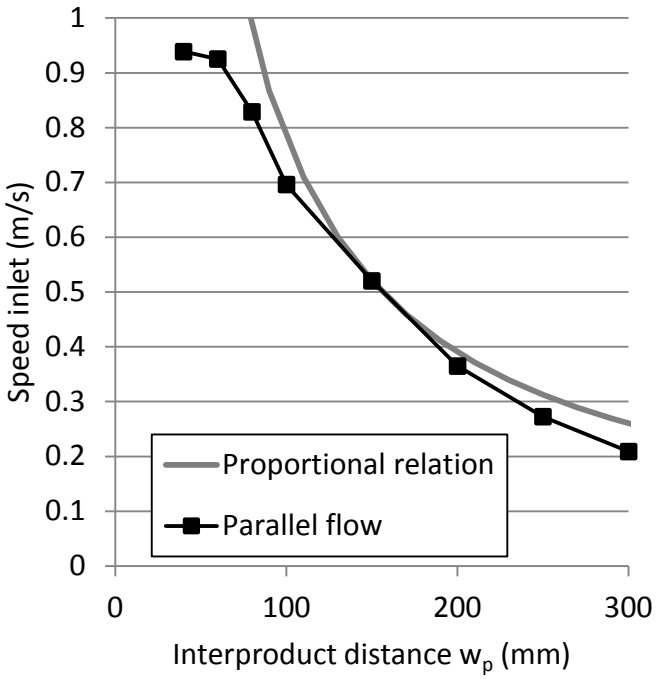

Figure 4. Average air speed at the domain inlet for flow around a product (parallel flow) for a periodic wire-to-mesh configuration, calculated for variable product spacing w_p.